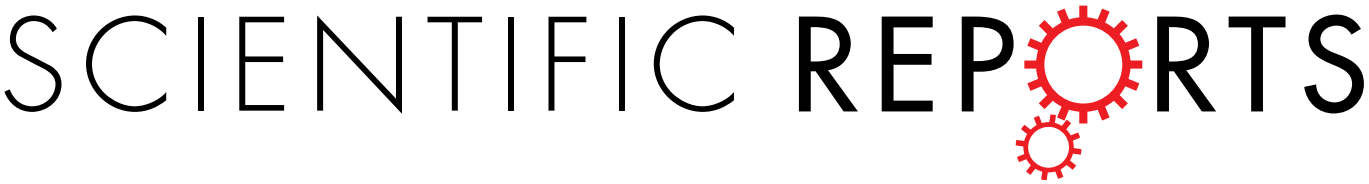

OPEN

Catalytic hydrolysis of carbonyl sulphide and carbon disulphide over Fe_2O_3 cluster: Competitive adsorption and reaction mechanism

Received: 12 June 2017
Accepted: 18 October 2017
Published online: 31 October 2017

Ping Ning[1], Xin Song[1], Kai Li[1], Chi Wang[2], Lihong Tang[1] & Xin Sun[1]

The competitive adsorption and reaction mechanism for the catalytic hydrolysis of carbonyl sulphide (COS) and carbon disulphide (CS_2) over Fe_2O_3 cluster was investigated. Compared with experimental results, the theoretical study was used to further investigate the competitive adsorption and effect of H_2S in the hydrolysis reaction of COS and CS_2. Experimental results showed that Fe_2O_3 cluster enhanced the catalytic hydrolysis effect. Meanwhile, H_2S was not conducive to the hydrolysis of COS and CS_2. Theoretical calculations indicated that the order of competitive adsorption on Fe_2O_3 is as follows: H_2O (strong) > CS_2 (medium) > COS (weak). In the hydrolysis process, the C=S bond cleavage occurs easier than C=O bond cleavage. The hydrolysis reaction is initiated via the migration of an H-atom, which triggers C=S bond cleavage and S–H bond formation. Additionally, we find the first step of CS_2 hydrolysis to be rate limiting. The presence of H_2S increases the reaction energy barrier, which is not favourable for COS hydrolysis. Fe_2O_3 can greatly decrease the maximum energy barrier, which decreases the minimum energy required for hydrolysis, making it relatively facile to occur. In general, the theoretical results were consistent with experimental results, which proved that the theoretical study was reliable.

As the by-products in the industrial production, such as closed carbide furnace tail gas, carbonyl sulphide (COS) and carbon disulphide (CS_2) corrode pipeline equipment and influence the purity of the raw material gas[1–6]. Currently, catalytic hydrolysis provided lower levels of by-products under mild reaction conditions and has thus become the most commonly used method to remove COS and CS_2 from industrial processes[7–12]. Several previous studies showed that Fe_2O_3 was suitable for catalytic hydrolysis of COS and CS_2[13–17]. In our previous study, different active components (such as Fe, Cu, Zn, Cr, Co, Ni) supported on AC were investigated for catalytic hydrolysis of COS and CS_2[13]. The results showed that Fe_2O_3/AC had the highest catalytic hydrolysis performance for COS and CS_2, yielding a 100% removal rate of CS_2 and COS after 330 min and 240 min respectively. For Fe_2O_3/AC, AC played a role of adsorbent and Fe_2O_3 played a role of active component. Furthermore, nano-Fe_2O_3/AC showed higher catalytic ability for CS_2, which prolonged 100% removal rate of CS_2 to 480 min[18]. However, the detailed reaction mechanisms are different for different catalysts and reaction paths. For instance, Guo *et al.* and Zhang *et al.* reported the COS hydrolysis mechanism without the use of a catalyst[19,20]. The results indicated that OH and H in H_2O first attack the C=O and C=S bonds in COS. Li *et al.* also investigated the COS hydrolysis mechanism. The results indicated that the nucleophilic additions of water across the C=O or C=S bonds of COS were competitive[21]. Additionally, the mechanism of CS_2 hydrolysis is identical to that of COS, and COS is an intermediate the hydrolysis of CS_2.

Currently, little research has focused on the reaction mechanism for the simultaneous removal of COS and CS_2. Although Fe_2O_3 was suitable for catalytic hydrolysis of COS and CS_2, the corresponding reaction mechanism remains unknown. Determining the detailed steps of the reaction mechanism is necessary because they can provide a theoretical foundation for the future application and development. Therefore, this work performed theoretical study to investigate the reaction mechanism and reaction routes of the simultaneous removal of COS

[1]Faculty of Environmental Science and Engineering, Kunming University of Science and Technology, Kunming, 650500, PR China. [2]Faculty of Chemical Engineering, Kunming University of Science and Technology, Kunming, 650500, PR China. Correspondence and requests for materials should be addressed to K.L. (email: likaikmust@163.com)

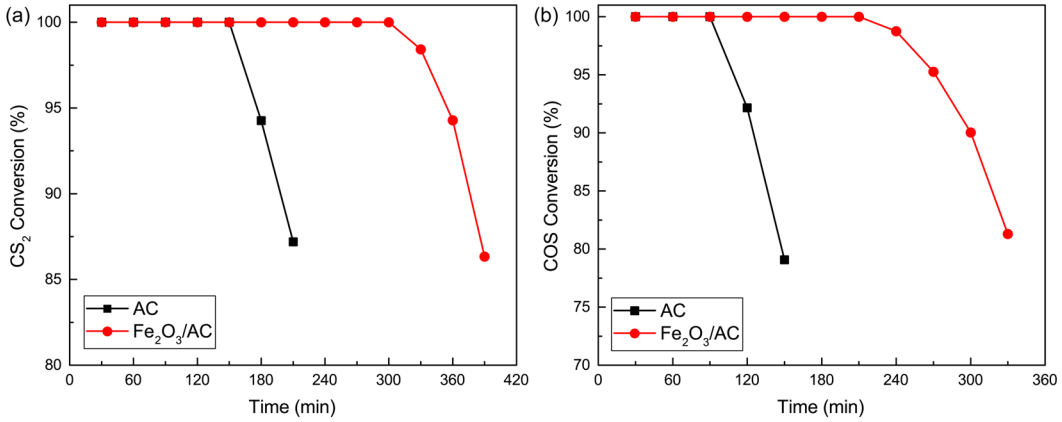

Figure 1. Simultaneous removal of (**a**) CS_2 and (**b**) COS over Fe_2O_3/AC and pure AC (Experimental conditions: 15 ppm CS_2; 500 ppm COS; GHSV = 10000 h^{-1}; reaction temperature: 70 °C; RH = 49%; O_2 = 0%; H_2S = 0%).

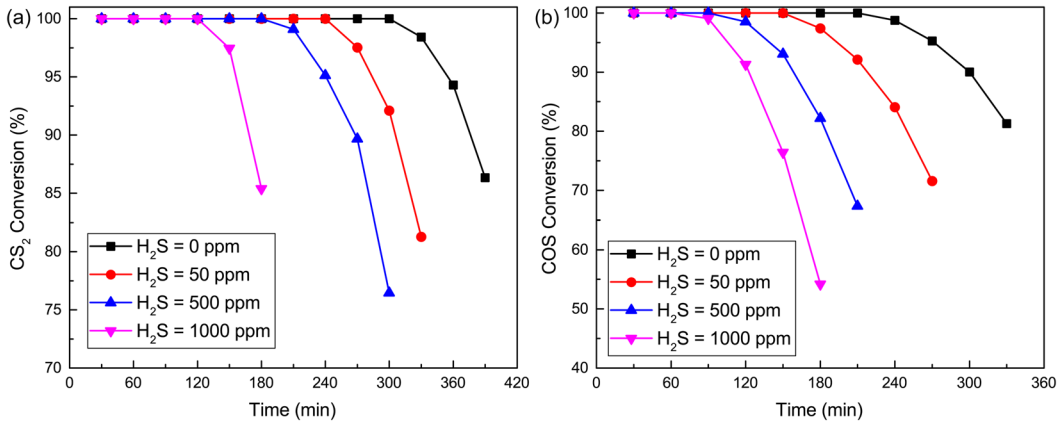

Figure 2. Simultaneous removal of (**a**) CS_2 and (**b**) COS over Fe_2O_3/AC at different inlet H_2S content (Experimental conditions: 15 ppm CS_2; 500 ppm COS; GHSV = 10000 h^{-1}; reaction temperature: 70 °C; RH = 49%; O_2 = 0%).

and CS_2 over Fe_2O_3 cluster. Combined with the experimental study, this theoretical study further investigated the competitive adsorption and effect of H_2S in the hydrolysis reaction of COS and CS_2.

Results and Discussion

Experimental study analysis. To provide the catalytic hydrolysis effect of Fe_2O_3, the desulphurization experiments for COS and CS_2 over Fe_2O_3/AC and pure AC were performed. The catalytic hydrolysis activities were showed in Fig. 1. From Fig. 1, the removal efficiency of COS and CS_2 over Fe_2O_3/AC were higher than that over pure AC. Addition of Fe_2O_3 cluster prolonged the 100% COS and CS_2 removal rate from 90 min to 210 min and 150 min to 300 min respectively. The effluent H_2S and CO_2 content over time was showed in Supplementary Fig. S1. As shown in Supplementary Fig. S1, the effluent H_2S content over Fe_2O_3/AC firstly increased and then decreased over time. Firstly, the hydrolysis reaction rate was fast. The generation rate of H_2S was higher than the adsorption rate, which led to the increase of H_2S. With the increase of reaction time, H_2S was gradually adsorbed on the surface of catalyst, which covered the active site of Fe_2O_3 cluster and adsorptive site of AC. As a result, it led to the deactivation of catalyst and the H_2S content decreased. Compared with Fe_2O_3/AC, the effluent H_2S content over pure AC was almost 0. Meanwhile, the CO_2 content over Fe_2O_3/AC was firstly almost stable and then decreased over time. The decrease of CO_2 content was attributed to the decrease of catalytic activity, which was caused by deactivation of catalyst. Compared with Fe_2O_3/AC, the effluent CO_2 content over pure AC was almost 0. These results indicated that the removal of CS_2 and COS over pure AC was mainly an adsorption process. Therefore, the removal of CS_2 and COS over Fe_2O_3 cluster was a catalytic hydrolysis process. It indicated that Fe_2O_3 cluster provide the catalytic hydrolysis effect and sharply enhanced the catalytic activity.

To investigate the effect of H_2S, the desulphurization experiments for COS and CS_2 over Fe_2O_3/AC were performed. The catalytic hydrolysis activities of Fe_2O_3/AC at different inlet H_2S content were shown in Fig. 2. From Fig. 2, when the content of H_2S in the inlet was 0%, the removal efficiency of COS and CS_2 over Fe_2O_3/AC was highest. Meanwhile, the removal efficiency of COS and CS_2 decreased with increasing H_2S content. It indicated that H_2S is not conducive to the hydrolysis of COS and CS_2.

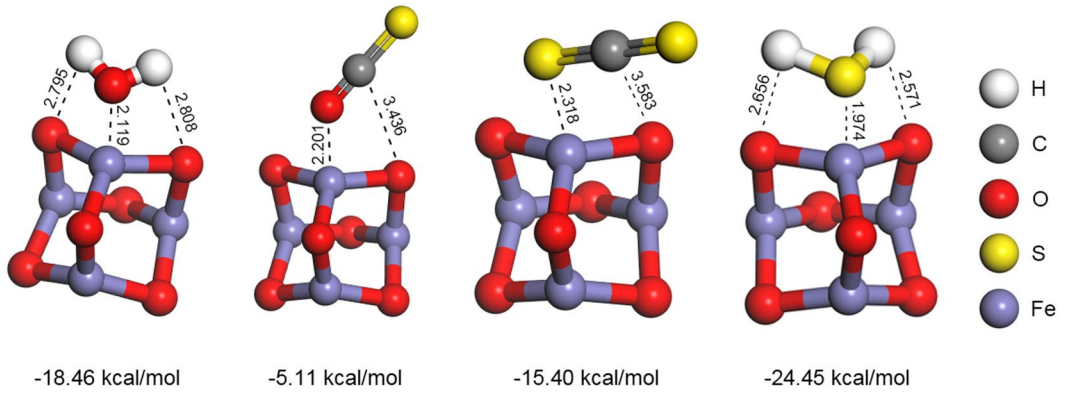

Figure 3. Optimized geometries and adsorption energies of H_2S, H_2O, COS and CS_2 over Fe_2O_3 (Adsorption energy, kcal/mol).

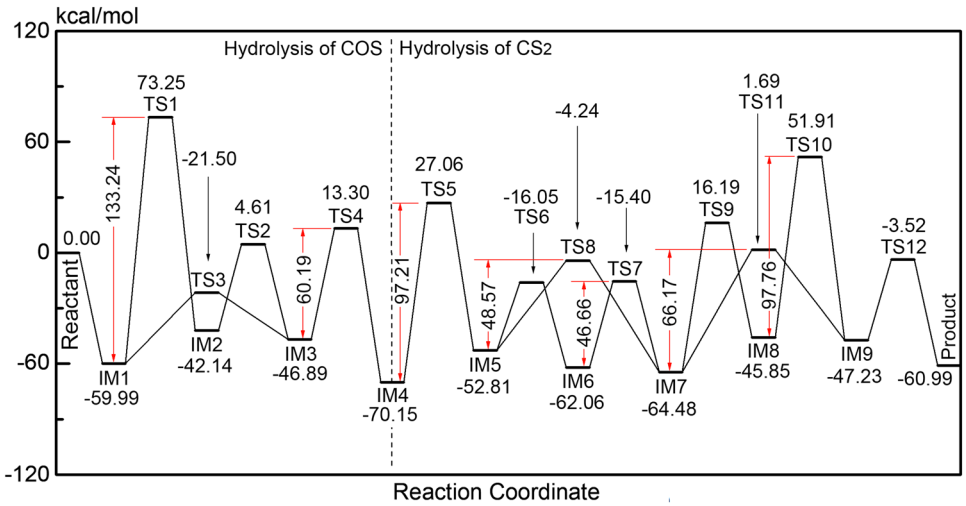

Figure 4. Reaction channel and potential energy surface for the hydrolysis of COS and CS_2 The optimized geometries for the hydrolysis of COS are presented in Fig. 5. The imaginary frequencies of the transition states are given in Supplementary Table S1.

To further investigate the effect of Fe_2O_3 and H_2S for the catalytic hydrolysis of COS and CS_2. The adsorption of COS and CS_2 on Fe_2O_3/AC and hydrolysis reaction mechanism were studied by theoretical calculation.

Theoretical study analysis. *Competitive adsorption analysis.* Because the size of nano-Fe_2O_3 structure was less than 10 nm and it had the cluster structure, the $(Fe_2O_3)_2$ cluster was used in the calculation study to represent the catalyst tested in experiments. To determine the relative (competitive) adsorption of H_2S, COS, CS_2 and H_2O, their corresponding optimized geometries and adsorption energies have been calculated (Fig. 3). As shown in Supplementary Fig. S2, when the O atom in COS pointed to surface Fe, the absolute value of the adsorption energy was lower. It might be attributed to that the adsorption effect of C-O…Fe was more stable than C-S…Fe. As shown in Fig. 3, for reactants, the absolute value of the adsorption energy of $H_2O + Fe_2O_3$ is the highest and that of $COS + Fe_2O_3$ is the lowest. These results indicate that H_2O is more easily adsorbed on the Fe_2O_3 cluster than COS and CS_2, which suggests that H_2O firstly adsorbs on the catalyst and then reacts with COS and CS_2. Meanwhile, the absolute value of the adsorption energy of $CS_2 + Fe_2O_3$ is the higher than that of $COS + Fe_2O_3$, which suggests that the adsorption of CS_2 on the surface of the catalyst occurs first. For the product H_2S, $H_2S + Fe_2O_3$ has higher absolute value of the adsorption energy than CS_2, COS and H_2O. It indicated that H_2S will be firstly adsorbed on the Fe_2O_3, which will gradually decrease the catalytic hydrolysis activity of catalyst.

Reaction mechanism of COS hydrolysis over Fe_2O_3 cluster. The reaction channels for the hydrolysis of COS and CS_2 are given in Fig. 4. The bond-lengths of transition states, reaction energies and energy barriers of various reaction steps were showed in Supplementary Table S1, Supplementary Table S2, Supplementary Table S3 and Supplementary Table S4. As seen in Fig. 4 and Supplementary Table S4, the energy barrier of COS hydrolysis (60.19 kcal/mol) over Fe_2O_3 is lower than that of CS_2 hydrolysis (97.21 kcal/mol), suggesting that the hydrolysis of COS occurs more easily than the hydrolysis of CS_2. Therefore, the hydrolysis of COS occurs preferentially for the simultaneous removal of COS and CS_2.

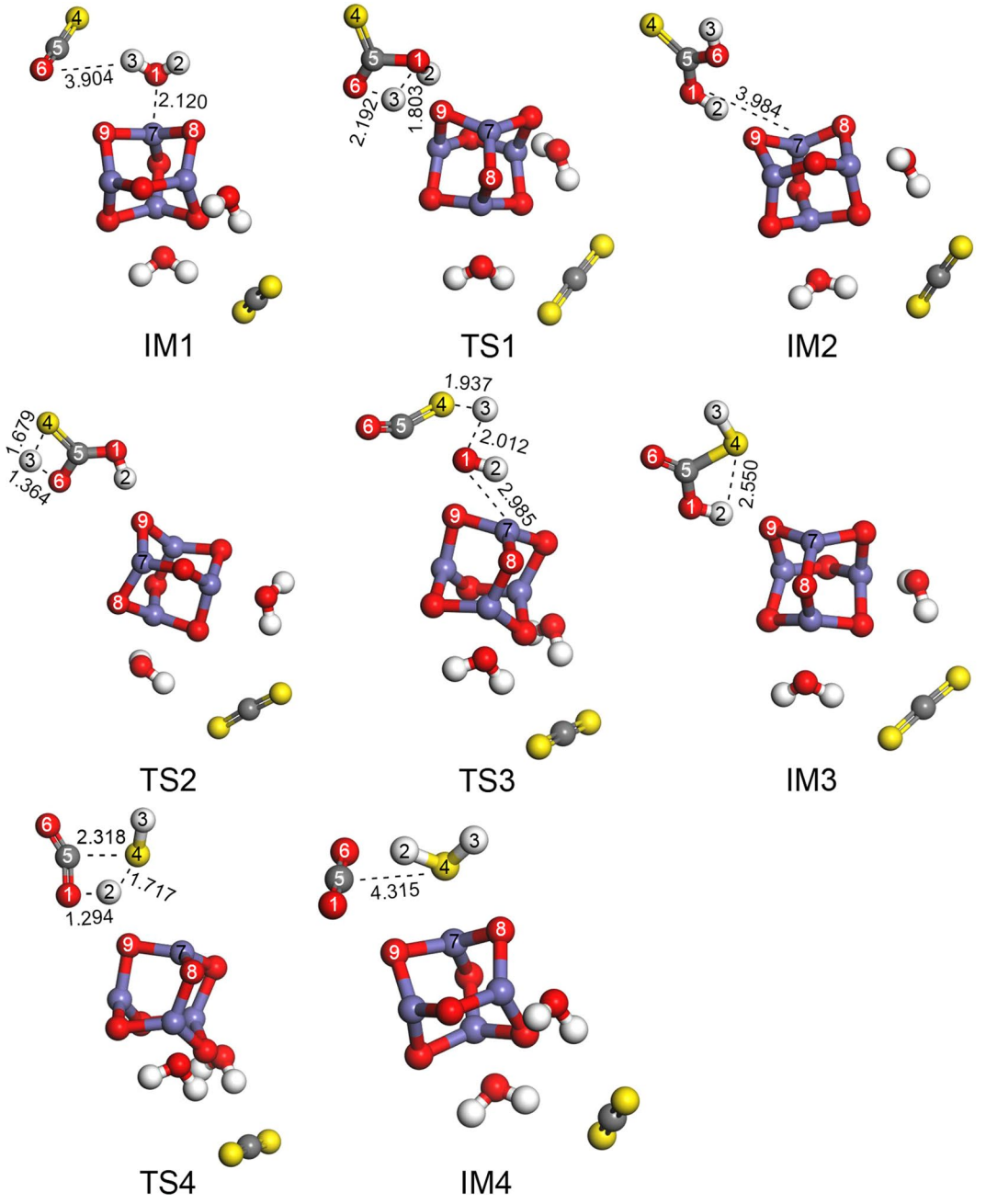

Figure 5. Optimized geometries (of IM and TS) for COS hydrolysis.

(1) C-O channel for COS hydrolysis.

In reaction channel I (i.e., Reactant → IM1 → TS1 → IM2 → TS2 → IM3 → TS4 → IM4), H_2O first adsorbs on the surface of Fe_2O_3, forming IM1. The C5–O1 bond length decreases and the H3–O1 bond breaks. At the same time, the C5–O1 and H3–O6 bonds are formed with the change from a C5=O6 double bond to a C5–O6 single bond to generate IM2 via TS1 (with just one imaginary frequency of –906.47 cm^{-1}). As seen in Fig. 5 and Supplementary Table S1, H3 moves from its position in IM1 to O6 in IM2 with an energy barrier of 133.24 kcal/mol. In effect, H3 and H2–O1 in H_2O attack the O6 and C5 atoms in COS, respectively.

The H3–O6 bond length then becomes longer as the H3–S4 bond length becomes shorter. Meanwhile, the H3–O6 bond breaks and the C5=O6 bond forms from the C5–O6 bond. Then, H3 migrated from the H3–O6 bond in IM2 to the H3–S4 bond in IM3. As the result, IM3 is generated via TS2 (with just one imaginary frequency of –1528.43 cm^{-1}) with an energy barrier of 46.75 kcal/mol. For TS2, Fe_2O_3 had an adsorption effect on O9 and H2, which led to that the migration of H3 from O6 to S4 was easier than H2 from O1 to S4.

Concomitantly, the bond lengths of H2–O1 and C5–S4 become longer and the H2–S4 bond length becomes shorter. Additionally, the H2–O1 and C5–S4 bonds become broken, the H2–S4 bond forms, and the C5=O1 bond forms from the C5–O1 bond. Subsequently, the products (IM4) are formed via TS4 (with just one imaginary

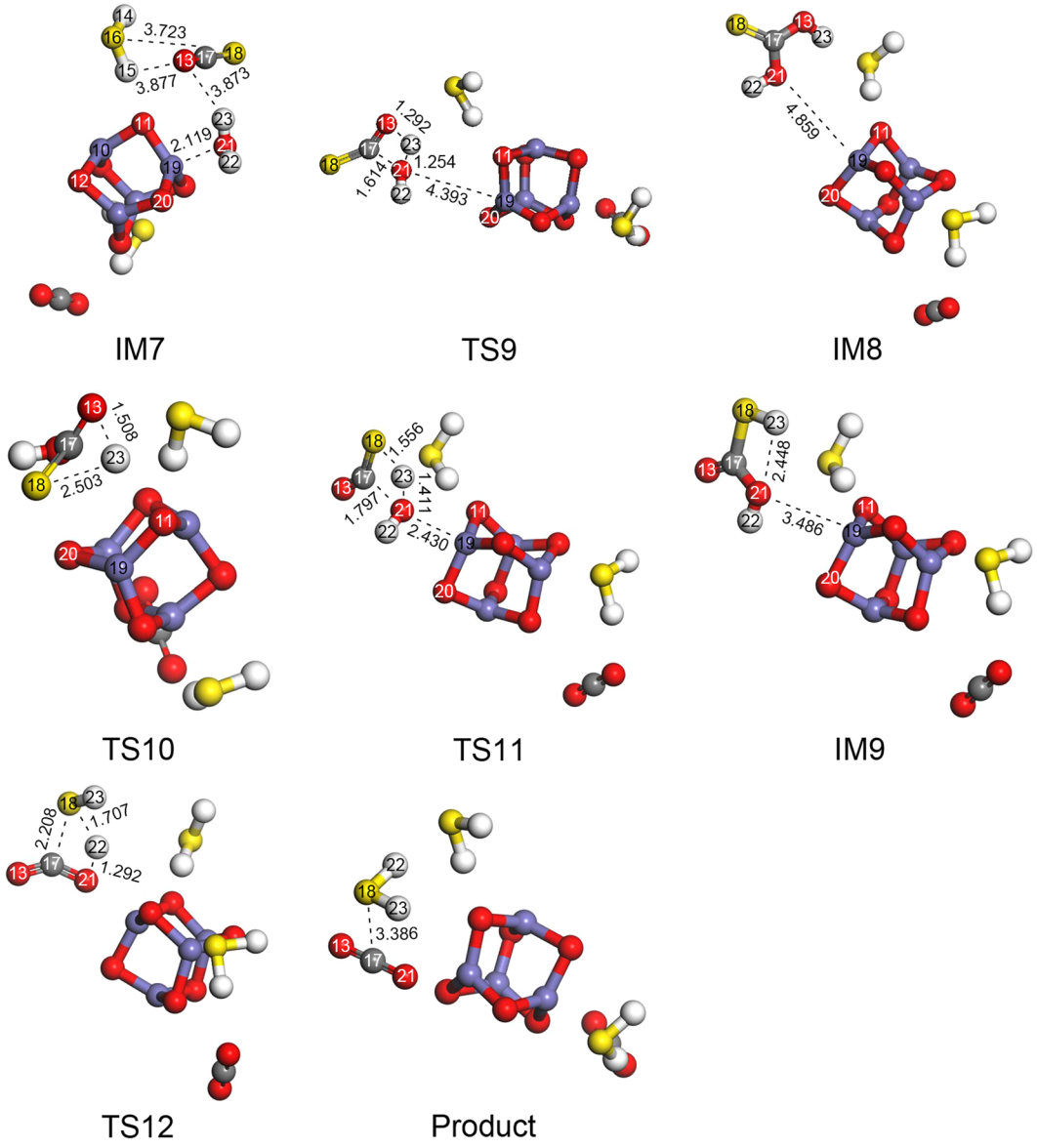

Figure 6. Optimized geometries (of IM and TS) for step 1 of CS_2 hydrolysis.

frequency of –1643.95 cm^{-1}) with an energy barrier of 60.19 kcal/mol. H2 migrated from the H2–O1 bond in IM3 to the H2–S4 bond in IM4.

(2) C-S channel for COS hydrolysis

In reaction channel II (i.e., Reactant → IM1 → TS3 → IM3 → TS4 → IM4), H_2O first adsorbs on the surface of Fe_2O_3 to generate IM1. Then, the C5–O1 bond length decreases and the H3–O1 bond breaks. At the same time, the C5–O1 and H3–S4 bonds form with the change from a C5=S4 double bond to a C5–S4 single bond, forming IM3 via TS3 (with just one imaginary frequency of −755.33 cm^{-1}). H3 moves from its position in IM1 to S4 in IM3 with an energy barrier of 38.49 kcal/mol. More specifically, H3 and H2–O1 in H_2O attack the S4 and C5 atoms in COS, respectively. For TS3, the adsorption effect of Fe7 and O1-H2 led to that the migration of H3 from O1 to H4 was easier than H2 from O1 to S4. The subsequent steps are identical to those in reaction channel I (i.e., IM3 → TS4 → IM4).

On the basis of these results, it is clear that the migration of H3 from the H3–O1 bond in IM1 to the H3–S4 bond in IM3 is easier than the migration of H3 from H3–O1 bond to the H3–O6 bond. Thus, the H–S bond forms more easily than the H–O bond, and reaction channel II is likely to occur more readily than reaction channel I.

Reaction mechanism of CS2 hydrolysis over Fe2O3 cluster. As seen in Fig. 4, the hydrolysis of CS_2 can be divided into two steps: CS_2 → COS and COS → H_2S. The optimized geometries for the step 1 of hydrolysis of CS_2 are presented in Fig. 6, and the imaginary frequencies of the transition states for COS hydrolysis are shown in Supplementary Table S2. The optimized geometries for the step 2 of hydrolysis of CS_2 are presented in Fig. 7, and the imaginary frequencies of the transition states for COS hydrolysis are shown in Supplementary Table S3.

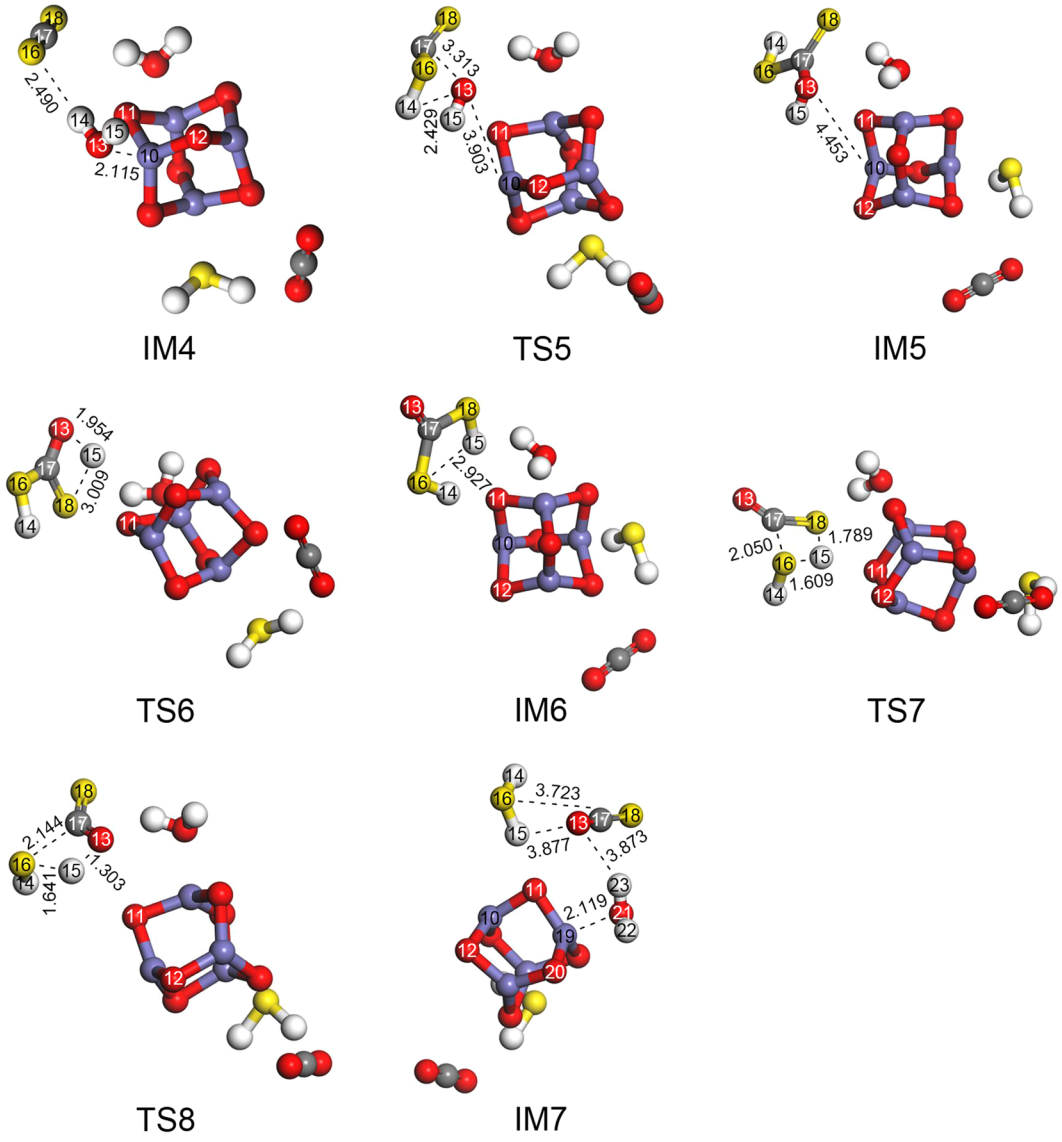

Figure 7. Optimized geometries (of IM and TS) for step 2 of CS_2 hydrolysis.

(1) Double H-S channel for step 1 of CS_2 hydrolysis.

In reaction channel III (i.e., the first step of CS_2 hydrolysis: IM4 → TS5 → IM5 → TS6 → IM6 → TS7 → IM7), the C17–O13 bond length decreases and the H14–O13 bond breaks. As a result, the C17–O13 and H14–S16 bonds form with the change from a C17=S16 double bond to a C17–S16 single bond to generate IM5 via TS5, which has only one imaginary frequency of $-703.92\,cm^{-1}$. As seen in Fig. 6 and Supplementary Table S2, H14 moves from its position in IM4 to S16 in IM5 with an energy barrier of 97.21 kcal/mol. Thus, H14 and H14–O13 in H_2O attack the S16 and C17 atoms in CS_2, respectively.

Consequently, the H15–O13 bond length becomes longer and the H15–S18 bond length becomes smaller. Meanwhile, the H15–O13 bond breaks and the C17=O13 bond forms from the C17–O13 bond. As a result, IM6 is generated via TS6 (with just one imaginary frequency of $-1045.81\,cm^{-1}$) with an energy barrier of 36.76 kcal/mol. H15 migrated from the H15–O13 bond in IM5 to the H15–S18 bond in IM6.

Concomitantly, the H15–S18 and C17–S16 bond lengths become longer while the H15–S16 bond length becomes smaller. Additionally, the H15–S18 and C17–S16 bonds break, the H15–S16 bond forms, and the C17=S18 bond is generated from the C17–S18 bond. Subsequently, IM7 is formed via TS7 (with just one imaginary frequency of $-1019.70\,cm^{-1}$) with an energy barrier of 46.66 kcal/mol. H15 migrated from the H15–S18 bond in IM6 to the H15–S16 bond in IM7.

(2) Single H-S channel for step 1 of CS_2 hydrolysis.

In reaction channel IV (i.e., the first step of CS_2 hydrolysis: IM4 → TS5 → IM5 → TS8 → IM7), IM5 is formed via TS5 causing the H15–O13 bond length to become longer and the H15–S16 bond length to become shorter. Meanwhile, the H15–O13 bond breaks and the C17=O13 bond forms from the C17–O13 bond. These changes

lead to IM7, which is generated via TS8 (with just one imaginary frequency of −1546.07 cm^{-1}) with an energy barrier of 48.57 kcal/mol. H15 migrated from the H15–O13 bond in IM5 to the H15–S16 bond in IM7.

Based on these results, the migration of H15 from the H15–O13 bond to the H15–O18 bond in IM6 occurs more easily than the migration of H15 from the H15–O13 bond in IM5 to the H15–S16 bond in IM7. Overall, these results suggest that the H atom more easily forms an H–S bond with the C=S bond than the C–S bond and that reaction channel III occurs more easily than reaction channel IV.

(3) C-O channel for step 2 of CS_2 hydrolysis.

As seen in Fig. 7, in reaction channel V (i.e., the second step of CS_2 hydrolysis: IM7 → TS9 → IM8 → TS10 → IM9 → TS12 → Product), the C17–O21 bond length decreases and the H23–O21 bond breaks. At the same time, the C17–O21 and H23–O13 bonds are formed with the change from C17=O13 to C17–O13, forming IM8 via TS9 (with just one imaginary frequency of −1624.81 cm^{-1}). As seen in Fig. 7 and Supplementary Table S3, H23 moves from its position in IM7 to O13 in IM8 with an energy barrier of 80.67 kcal/mol, and H23 and H23–O21 in H_2O attack the O13 and C17 atoms in COS, respectively.

The H23–O13 bond length then becomes longer while the H23–S18 bond length becomes shorter. Meanwhile, the H23–O13 bond breaks and the C17=O13 bond forms from the C17–O13 bond. Then, H23 migrated from the H23–O13 bond in IM8 to the H23–S18 bond in IM9. As the result, IM9 is generated via TS10 (with just one imaginary frequency of −1325.24 cm^{-1}) with an energy barrier of 97.76 kcal/mol.

Concomitantly, the H22–O21 and S18–C17 bond lengths become longer while the H22–S18 bond length becomes shorter. Additionally, the H22–O21 and C17–S18 bonds break, the H22–S18 bond forms, and the C17=O21 bond forms from the C17–O21 bond. Subsequently, the products are formed via TS12 (with just one imaginary frequency of −1495.37 cm^{-1}) with an energy barrier of 43.71 kcal/mol. H22 migrated from the H22–O21 bond in IM9 to the H22–S18 bond in the product.

(4) C-S channel for step 2 of CS_2 hydrolysis.

In reaction channel VI (i.e., the second step of CS_2 hydrolysis: IM7 → TS11 → IM9 → TS12 → Product), the C17–O21 bond length decreases and the H23–O21 bond breaks. At the same time, the C17–O21 and H23–O18 bonds are formed with the change from C17=S18 to C17–S18, forming IM9 via TS11 (with just one imaginary frequency of −1172.61 cm^{-1}). As seen, H23 moves from its position in IM7 to S18 in IM9 with an energy barrier of 66.17 kcal/mol, and H23 and H22–O21 in H_2O attack the S18 and C17 atoms in COS, respectively. The subsequent steps are then identical to those in reaction channel V (IM9 → TS12 → Product).

Overall, it is clear that the migration of H23 from the H23–O21 bond in IM7 to the H23–S18 bond in IM9 occurs more easily than the migration of H23 from the H23–O21 bond to the H23–O13 bond. The results also indicate that the H–S bond forms more easily than the H–O bond, which agrees with the above results. Therefore, reaction channel VI is likely to occur more easily than reaction channel V.

Effect of H_2S and Fe_2O_3 on hydrolysis of CS_2 and COS. According to the above results, the order of the competitive adsorption on Fe_2O_3 is as follows: H_2O (strong) > CS_2 (medium) > COS (weak). H_2S does not change the priority of the migration of the H atom in H_2O from the H–O bond to the H–S bond. In the hydrolysis, the C=S bond cleavage occurs easier than C=O bond cleavage. The presence of H_2S increases the maximum energy barrier for COS hydrolysis (from 60.19 kcal/mol to 66.17 kcal/mol), which was attributed to the competitive adsorption effect. As the result, it covered the active sites and was not favourable for COS hydrolysis. Meanwhile, the first step of CS_2 hydrolysis has a higher energy barrier than the second step, which indicates that the first step is rate-limiting. The energy barriers of gas-phase reaction were showed in Supplementary Table S5. Compared with gas-phase reaction without catalyst, all the maximum energy barriers of surface reaction were lower. The addition of Fe_2O_3 can greatly decrease the maximum energy barrier (159.74 kcal/mol and 182.71 kcal/mol for COS and CS_2, respectively), which decreases the minimum energy required for the hydrolysis reaction. It was attributed to the adsorption effect between Fe_2O_3 and H_2O, and H migration. From the experimental results, nano-Fe_2O_3 cluster promoted the catalytic hydrolysis reaction of CS_2 and COS. It might be attributed to the interaction effect Fe_2O_3 and COS/CS_2, and high catalytic hydrolysis activity of Fe_2O_3. As a product, H_2S decreased the removal efficiency of COS and CS_2 when it was on the surface of catalyst. It indicated that H_2S was not conducive to the hydrolysis of COS and CS_2. The results demonstrate that Fe_2O_3 is a good catalyst for the hydrolysis of COS and CS_2. In general, theoretical results were consistent with experimental results, which proved that the theoretical study was reliable. Combined with theoretical and experimental results, it can be found that the influence mechanism of Fe_2O_3 and H_2S for catalytic hydrolysis of COS and CS_2.

Conclusions

The competitive adsorption and reaction mechanism for the catalytic hydrolysis reaction mechanism of carbonyl sulphide (COS) and carbon disulphide (CS_2) over Fe_2O_3 cluster was investigated in this work. The experimental results showed that Fe_2O_3 cluster enhanced the catalytic hydrolysis effect. Meanwhile, H_2S was not conducive to the hydrolysis of COS and CS_2. On the basis of the calculation results, the order of competitive adsorption on Fe_2O_3 is: H_2O (strong) > CS_2 (medium) > COS (weak). In the hydrolysis process, the C=S bond cleavage occurs easier than C=O bond cleavage. The presence of H_2S increases the reaction energy barrier, which is not favourable for COS hydrolysis. Meanwhile, Fe_2O_3 can greatly decrease the maximum energy barrier, which decreases the minimum energy required for hydrolysis, making it relatively facile to occur. Combined with theoretical and experimental results, it can be found that the influence mechanism of Fe_2O_3 and H_2S for catalytic hydrolysis of COS and CS_2.

Experimental and Theoretical Methods

Experimental Methods. To investigate the effect of nano-Fe_2O_3 cluster for catalytic hydrolysis of COS and CS_2, AC (activated carbon) and nano-Fe_2O_3 cluster/AC were used in this work. Nano-Fe_2O_3 cluster was

synthesized by hydro-thermal method[22]. 4.40 g $FeCl_3$ and 4.0 g urea were added into 100 mL distilled water. 50 mL $NH_3{\cdot}H_2O$ was added dropwise into the solution with continuous magnetic stirring. The solution was poured into a Teflon-lined container and then it was heated at 150 °C for 12 h. The solution was cooled under room temperature. The obtained precipitates were washed by ethanol and distilled water for three times. Finally, the precipitates were calcinated at 450 °C for 3 h. The size of nano-Fe_2O_3 structure was less than 10 nm and it had the cluster structure. Nano-Fe_2O_3 cluster/AC (activated carbon) was synthesized by dipping method according to our previous study[13,14]. 5% mass content of nano-Fe_2O_3 cluster and AC were added into 50 mL distilled water. The solution was placed in an ultrasonic bath for 30 min. Finally, the solution was dried at 120 °C for 20 h and nano-Fe_2O_3 cluster/AC was prepared.

The desulphurization tests were performed in a fixed–bed quartz reactor under atmospheric pressure[13,14]. CS_2 and COS from the gas cylinder (0.3% CS_2 in N_2; 1% COS in N_2) were diluted with N_2 (99.99%) to the required concentration (CS_2: 20 ppm; COS: 500 ppm). The overall gas hourly space velocity (GHSV) was 10000 h^{-1}. Water was obtained from a saturator system, which set the temperature and corresponding relative humidity (RH) to 5 °C and 49%, respectively. The temperature of the reactor was maintained at 70 °C using a water bath. The CS_2, COS and H_2S (hydrolysis product) concentration of the gas feed and effluent from the reactor were analysed using a HC–6 sulphur phosphorus microscale analyser. The removal rate of CS_2 and COS were determined by calculating the inlet and outlet concentration of CS_2 and COS, and it was shown in Eq. 1:

$$CS_2(COS)\text{conversion }(\%) = \frac{CS_2(COS)_{in} - CS_2(COS)_{out}}{CS_2(COS)_{in}} \times 100 \quad (1)$$

Theoretical Methods. All calculations in this work were performed using Dmol[3] in the Material Studio software package[23]. The molecular geometries of the reactants, transition states (TS), intermediate complexes (IM), and products were calculated and optimized using the GGA/PBE method from density functional theory (DFT)[24,25]. A density functional semi-core pseudopotential method was used for the core electrons of Fe, and the all-electron method was used for the core electrons of H, C, O and S. A double-numeric quality basis set with polarization functions (i.e., DNP, version 3.5) was used[25–27]. The tolerances of the SCF, energy, gradient and displacement convergence were 1.0×10^{-6} hartree (Ha), 1.0×10^{-5} Ha, 2.0×10^{-3} Ha/Å and 5.0×10^{-3} Å, respectively. All calculations using spin-polarized set were performed considering the antiferromagnetic properties. In previous study, electronic self-interaction error played an important role in DFT[28,29]. Therefore, the electron self-interaction error had been consideration in this work. Self-consistent field convergence was declared when at least two of the above criteria were satisfied. Electronic energies and zero point vibration energies (ZPVE) were calculated at the same level of theory. Linear synchronous transit/quadratic synchronous transit/conjugate gradient (LST/QST/CG) calculations were used to ensure that all of the transition states connected to the intended reactants and products. Transition states were identified by the presence of a single imaginary frequency, which corresponded to the reaction mode. The adsorption energy was defined as Eq. 2. $E_{(adsorbate+cluster)}$ is the total energy of adsorbate/cluster system after gas molecule being adsorbed on Fe_2O_3 cluster. $E_{adsorbate}$ is the single-point energy of gas molecule and $E_{cluster}$ is the single-point energy of Fe_2O_3 cluster.

$$E_{ads} = E_{(adsorbate+cluster)} - E_{adsorbate} - E_{cluster} \quad (2)$$

References

1. Leman, L. J., Orgel, L. E. & Ghadiri, M. R. Amino acid dependent formation of phosphate anhydrides in water mediated by carbonyl sulfide. *J. Am. Chem. Soc.* **128**, 20–21 (2006).
2. Sun, X. *et al.* Simultaneous catalytic hydrolysis of carbonyl sulfide and carbon disulfide over Al_2O_3-K/CAC catalyst at low temperature. *J. Energy Chem.* **23**, 221–226 (2014).
3. Chowanietz, V., Pasel, C. H. R., Eckardt, T., Siegel, A. & Bathen, D. Formation of carbonyl sulfide (COS) on different adsorbents in natural gas treatment plants. *Oil Gas-Eur. Mag.* **42**, 82–85 (2016).
4. Zhao, S. Z. *et al.* Enhancement effects of ultrasound assisted in the synthesis of NiAl hydrotalcite for carbonyl sulfide removal. *Ultrason. Sonochem.* **32**, 336–342 (2016).
5. Qiu, J. *et al.* Removing carbonyl sulfide with metal-modified activated carbon. *Front. Env. Sci. Eng.* **10**, 11–18 (2016).
6. Kuznetsov, D. L., Filatov, I. E. & Uvarin, V. V. Processes of carbon disulfide degradation under the action of a pulsed corona discharge. *Tech. Phys. Lett.* **42**, 822–825 (2016).
7. Yegiazarov, Y. *et al.* Adsorption-catalytic process for carbon disulfide removal from air. *Catal. Today* **102–103**, 242–247 (2005).
8. Huang, H., Young, N., Williams, B. P., Taylor, S. H. & Hutchings, G. High temperature COS hydrolysis catalysed by γ-Al_2O_3. *Catal. Lett.* **110**, 243–246 (2006).
9. Liu, Y., He, H. & Ma, Q. Temperature dependence of the heterogeneous reaction of carbonyl sulfide on magnesium oxide. *J. Phys. Chem. A* **112**, 2820–2826 (2008).
10. Rhodes, C., Riddel, S. A., West, J., Williams, B. P. & Hutchings, G. J. The low-temperature hydrolysis of carbonyl sulfide and carbon disulfide: a review. *Catal. Today* **59**, 443–464 (2000).
11. Ning, P. *et al.* Effect of Fe/Cu/Ce loading on the coal-based activated carbons for hydrolysis of carbonyl sulfide. *J. Rare Earth.* **28**, 205–210 (2010).
12. Yang, Y., Shi, Y. & Cai, N. Simultaneous removal of COS and H_2S from hot syngas by rare earth metal-doped SnO_2 sorbents. *Fuel* **181**, 1020–1026 (2016).
13. Song, X. *et al.* Research on the low temperature catalytic hydrolysis of COS and CS_2 over walnut shell biochar modified by Fe–Cu mixed metal oxides and basic functional groups. *Chem. Eng. J.* **314**, 418–433 (2017).
14. Li, K. *et al.* Energy Utilization of yellow phosphorus tail gas: simultaneous catalytic hydrolysis of carbonyl sulfide and carbon disulfide at low temperature. *Energy Technol.* **3**, 136–144 (2015).
15. Ning, P. *et al.* Simultaneous catalytic hydrolysis of carbonyl sulfide and carbon disulfide over modified microwave coal-based active carbon catalysts at low temperature. *J. Phys. Chem. C* **116**, 17055–17062 (2012).
16. Yi, H. *et al.* Simultaneous catalytic hydrolysis of low concentration of carbonyl sulfide and carbon disulfide by impregnated microwave activated carbon at low temperatures. *Chem. Eng. J.* **230**, 220–226 (2013).

17. Li, K. *et al*. Surface modification of Fe/MCSAC catalysts with coaxial cylinder dielectric barrier discharge plasma for low-temperature catalytic hydrolysis of CS_2. *Appl. Catal. A* **527**, 171–181 (2016).
18. Li, K. *et al*. Low temperature catalytic hydrolysis of carbon disulfide over nano-active carbon based catalysts prepared by liquid phase deposition. *RSC Adv.* **7**, 40354–40361 (2017).
19. Guo, H. *et al*. The hydrolysis mechanism and kinetic analysis for COS hydrolysis: A DFT study. *Russ. J. Phys. Chem. B* **10**, 427–434 (2016).
20. Zhang, R. G., Ling, L. X. & Wang, B. J. Density functional theory analysis of carbonyl sulfide hydrolysis: effect of solvation and nucleophile variation. *J. Mol. Model.* **18**, 1255–1262 (2012).
21. Li, X.-H. *et al*. Concerted or stepwise mechanism? new insight into the water-mediated neutral hydrolysis of carbonyl sulfide. *J. Phys. Chem. A* **118**, 3503–3513 (2014).
22. Jaafarzadeh, N., Ghanbari, F. & Ahmadi, M. Catalytic degradation of 2,4-dichlorophenoxyacetic acid (2,4-D) by nano-Fe_2O_3 activated peroxymonosulfate: Influential factors and mechanism determination. *Chemosphere* **169**, 568–576 (2017).
23. Perdew, J. P., Burke, K. & Ernzerhof, M. Generalized Gradient Approximation Made Simple. *Phys. Rev. Lett.* **77**, 3865–3868 (1996).
24. Delley, B. From molecules to solids with the DMol^3 approach. *J. Chem. Phys.* **113**, 7756–7764 (2000).
25. Delley, B. An all-electron numerical method for solving the local density functional for polyatomic molecules. *J. Chem. Phys.* **92**, 508–517 (1990).
26. Bethune, D. S., Williams, M. D. & Luntz, A. C. Laser IR polarization spectroscopy at surfaces. *J. Chem. Phys.* **88**, 3322–3330 (1988).
27. Barth, U. V. & Hedin, L. A local exchange-correlation potential for the spin polarized case. i. *J. Phys. C* **5**, 1629–1642 (1972).
28. Grafenstein, J. & Cremer, D. The self-interaction error and the description of non-dynamic electron correlation in density functional theory. *Theor. Chem. Acc.* **123**, 171–182 (2009).
29. Tobias, S. & Stephan, K. One- and many-electron self-interaction error in local and global hybrid functionals. *Phys. Rev. B* **93**, 165120-1–165120-15 (2016).

Acknowledgements

This work was supported by National Natural Science Foundation [51408282, 21667015 and 51708266], China Scholarship Council [201508530017, 201608530169 and 201608740011] and the Analysis and Testing Foundation of Kunming University of Science and Technology.

Author Contributions

Kai Li, Xin Song and Ping Ning revised the manuscript. Kai Li and Ping Ning conceived the ideas. Xin Song and Chi Wang wrote the main manusript text. Xin Song and Lihong Tang did the theoretical calculations and prepared Figures 3–7. Xin Song and Xin Sun did the desulphurization experiments and prepared Figures 1–2. Kai Li, Ping Ning and Xin Song offered the funds and prepared Tables S1–S3.

Additional Information

Supplementary information accompanies this paper at https://doi.org/10.1038/s41598-017-14925-5.

Competing Interests: The authors declare that they have no competing interests.

Publisher's note: Springer Nature remains neutral with regard to jurisdictional claims in published maps and institutional affiliations.